Inorganic Chemistry

Article

pubs.acs.org/IC

Multi-Center Redox-Active System: Amine−Amine Electronic Coupling through a Cyclometalated Bisruthenium Segment

Chang-Jiang Yao, Yu-Wu Zhong,* and Jiannian Yao

Beijing National Laboratory for Molecular Sciences, CAS Key Laboratory of Photochemistry, Institute of Chemistry, Chinese Academy of Sciences, Beijing 100190, China

University of Chinese Academy of Sciences, Beijing 100049, China

Supporting Information

ABSTRACT: A multicenter redox-active system with a linear N−Ru−Ru−N array, where two distal triarylamine sites are bridged by a cyclometalated bisruthenium segment, has been synthesized and characterized with single-crystal X-ray analysis. This system displays four consecutive and separate anodic redox waves at low potentials, indicating the presence of amine−amine electronic coupling with a distance of 19.16 Å through the cyclometalated bisruthenium segment. In contrast, when a noncyclometalated bisruthenium bridge is used, no amine−amine coupling is present. Upon stepwise oxidation by chemical or electrochemical methods, four-step absorption spectral changes occur in the visible to near-infrared region. In addition, the EPR studies and DFT and TDDFT calculations of the singly oxidized state are presented.

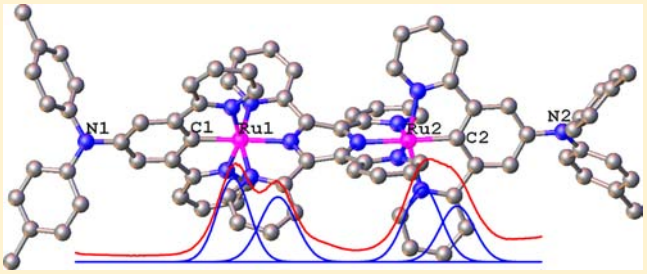

INTRODUCTION

The construction of one-dimensional materials with multiple (≥3) redox-active centers and multielectron redox processes at low operational potentials remains a challenging task.[1] These materials are very useful in fields such as molecular electronics,[2] charge-storage memory,[3] and photoconversion of solar energy.[4] Two-center molecular arrays with the general formula $[M^1-BL-M^2]^{n\pm}$ (M = redox-active sites, BL = bridging ligand) are the subject of a large body of work,[5] since the disclosure of the Creutz−Taube ion.[6] These systems include symmetric ($M^1 = M^2$) and nonsymmetric ($M^1 \neq M^2$) structures and both centers can either be an inorganic or a purely organic redox component.[5] However, linear systems with multiple centers and strong electronic coupling among individual components are limited.[1]

Bis-tridentate *cyclometalated* ruthenium complexes with the general formula $[(NNN)Ru(NCN)]^+$ contain a noncyclometalating NNN ligand and a cyclometalating NCN ligand.[7] Because of the presence of the σ-donating anionic carbon ligand, the $Ru^{II/III}$ process of such complexes takes place at a considerably lower potential with respect to *noncyclometalated* complexes $[Ru(NNN)_2]^{2+}$.[8] Besides, the pincer structure of the NCN ligand greatly stabilizes the complex. These features make cyclometalated ruthenium complexes very useful in dye-sensitized solar cells[9] and mixed-valence (MV) chemistry.[10] In conjugation with our ongoing projects on the synthesis and electronic coupling studies of symmetric cyclometalated bisruthenium complexes[11] and bis-triarylamine systems,[12] we have recently reported on the nonsymmetric MV system $\mathbf{1}^{n+}$ (Figure 1) composed of mixed inorganic (Ru) and organic (amine) redox-active species.[13] This complex displays two well-defined redox couples at +0.27 and +0.68 V vs Ag/AgCl. According to the electrochemical, spectroscopic, electron paramagnetic resonance (EPR), and theoretical studies, the first wave is ascribed to the $N/N^{\bullet+}$ process and the second to the $Ru^{II/III}$ process.[13] The low $N/N^{\bullet+}$ potential is a result of the strong electron delocalization and the inductive effect of the ruthenium component. The presence of the strong ruthenium-amine coupling is supported by the appearance of the narrow and intense Ru → N^+ metal-to-nitrogen charge transfer (MNCT) transitions at 1050 nm (in CH_3CN) in the MV state $\mathbf{1}^{2+}$. Herein, we present a new multicenter redox-active system $\mathbf{2}^{n+}$ and $\mathbf{3}^{n+}$ (Figure 1), which consist of two amine and two *cyclometalated* ruthenium centers with the two distal amine sites bridged by the linear bisruthenium component. This system displays four consecutive one-electron redox processes at low positive potentials, indicating the presence of electronic coupling between two distal amine sites.

RESULTS AND DISCUSSION

Synthesis and Single-Crystal Structure. Complexes $\mathbf{2}^{2+}$ and $\mathbf{3}^{2+}$ were prepared from the complexation of $[RuCl_3(tppz)RuCl_3]$[14] (tppz = tetra(2-pyridyl)pyrazine) with 1-(di-*p*-anisylamino)-3,5-di(2-pyridyl)benzene[13] or 1-(di-*p*-tolylamino)-3,5-di(2-pyridyl)benzene in the presence of AgOTf, followed by anion exchange using KPF_6. In addition, a model complex $\mathbf{4}^{4+}$ with two distal triarylamine units bridged by a *noncyclometalated* bisruthenium segment (Figure 1) was prepared from $[RuCl_3(tppz)RuCl_3]$ and 4′-di-*p*-anisylamino-

Received: January 12, 2013
Published: March 18, 2013

dx.doi.org/10.1021/ic400082z | Inorg. Chem. 2013, 52, 4040−4045

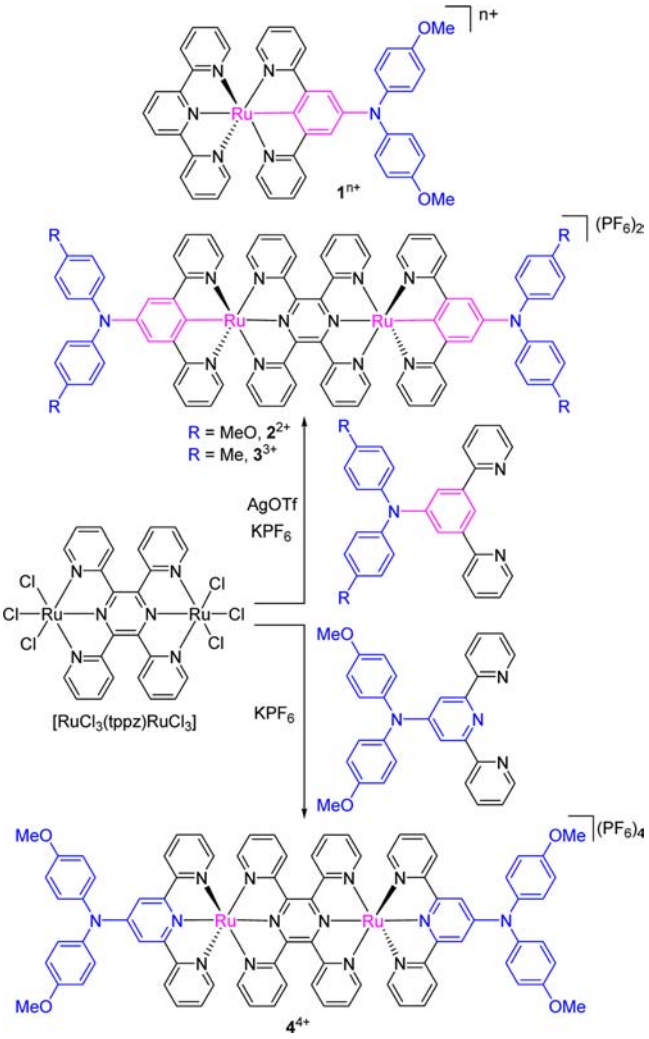

Figure 1. Compounds studied in this paper. Counter anions are PF_6^- if otherwise noted.

2,2′:6′,2″-terpyridine.[12c] The details and characterization data are given in the Experimental Section. The MALDI mass spectrometry (MS) spectra show signals corresponding to losses of two PF_6 anions of $[\mathbf{2}](PF_6)_2$ and $[\mathbf{3}](PF_6)_2$ and three anions of $[\mathbf{4}](PF_6)_3$ (1506.8, 1443.2, and 1653.0 D, respectively). No clear ^{1}H NMR spectra have been obtained for $\mathbf{2}^{2+}$ and $\mathbf{3}^{2+}$, possibly due to the presence of small amounts of paramagnetic species. However, the purity of the samples is supported by microanalysis data and following electrochemical analysis.

In the beginning, we failed to obtain single crystals from the above prepared complexes. Being ware of the fact that the counteranions PF_6^- are much smaller in size relative to their cationic bisruthenium component, we turned our attention to the bulky anion BPh_4^-. Fortunately, a single crystal of $[\mathbf{3}](BPh_4)_2$, which was generated after anion exchange with $[\mathbf{3}](PF_6)_2$, was obtained by diffusion of ethyl ether into a solution in CH_3CN. The thermal ellipsoid plot of the X-ray structure is shown in Figure 2. Each ruthenium atom has an octahedral configuration and two tridentate ligands around each ruthenium atom are orthogonal to each other. The two nitrogen atoms have a distance of 19.16 Å. The two ruthenium atoms have a distance of 6.74 Å. The two Ru−C bonds have the same length of 1.96 Å. The Ru−$N_{pyrazine}$ bond opposite to

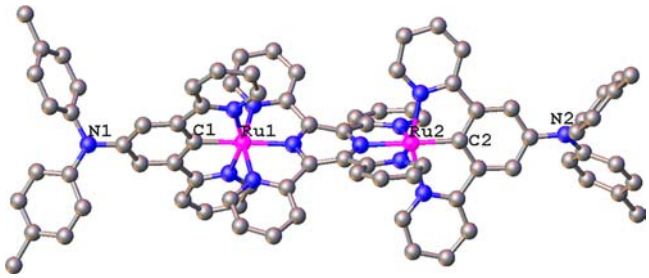

Figure 2. Thermal ellipsoid plot of the single-crystal structure of $[\mathbf{3}](BPh_4)_2$ with 30% probability. Hydrogen atoms and anions are omitted for clarity. Atom color code: carbon, gray; nitrogen, blue; ruthenium, magenta. Selected bond length: N1−N2, 19.16 Å; Ru1−Ru2, 6.74 Å.

the Ru−C bond has a length of 2.02 Å. Other Ru−N bonds are in the range of 2.05−2.11 Å. Similar geometrical distances have been reported for some monometallic cyclometalated ruthenium complexes.[8,15] The central tppz ligand has a distorted structure and the torsion angle between two side pyridine planes are 22.9° (Figure S1 in the Supporting Information, SI).

Electrochemical Study. Electrochemistry is frequently employed to study the electronic coupling between redox-active centers of symmetric $[M-BL-M]^{n\pm}$ systems. The appearance of a two-electron single redox wave is indicative of zero electronic coupling. On the other hand, two separated sequential redox waves point to the presence of an electronic coupling between redox sites. However, this principle should be taken with great care, because the electrochemical data are largely dependent on the measurement conditions, such as the solvent and supporting electrolyte used. The anodic cyclic voltammogram (CV) and differential pulse voltammogram (DPV) of complex $\mathbf{2}^{2+}$ shows four well-separated one-electron redox couples at +0.38, +0.48, +0.83, and +0.91 V vs Ag/AgCl in CH_3CN in the presence of the weakly coordinating electrolyte[16] ^{n}Bu$_4$NB$(C_6F_5)_4$ (Figure 3a and Table 1). By comparing with the electrochemical data of complex $\mathbf{1}^{n+}$,[13] it is reasonable to assign the first two waves of $\mathbf{2}^{2+}$ to the stepwise oxidations of two amine sites and the last two waves to the oxidations of ruthenium components. When the electrochemical measurement was carried out with a more conventional electrolyte, ^{n}Bu$_4$NClO$_4$, the last two waves are less resolved (Figure S2, Supporting Information). However, the stepwise oxidations of the amine sites are equally clear (+0.36 and +0.46 V). This indicates that the 100 mV separation of the two $N/N^{\bullet+}$ waves is not caused by the ion-pairing effects associated with the counterions of electrolytes,[16] but instead is a result of the electronic coupling between two distal amine sites. The comproportionation constant K_c for the singly oxidized state $\mathbf{2}^{3+}$ is 50 at room temperature, as determined by the equation $K_c = 10^{\Delta E\ (\mathrm{mV})/59.5}$.

The cathodic scan of $\mathbf{2}^{2+}$ shows two tppz-associated reduction waves at −0.70 and −1.14 V vs Ag/AgCl (Supporting Information Figure S3). Complex $\mathbf{3}^{2+}$ displays similar four anodic waves at +0.42, +0.54, +0.83, and +0.91 V vs Ag/AgCl in the presence of ^{n}Bu$_4$NClO$_4$ (Supporting Information Figure S4) as has been observed for complex $\mathbf{2}^{2+}$. The slightly positive shift of these waves relative to $\mathbf{2}^{2+}$ is reasonable because the substituents on the amine sites of $\mathbf{3}^{2+}$ are less electron-donating than those of $\mathbf{2}^{2+}$ (tolyl vs anisyl).

In contrast, complex $\mathbf{4}^{4+}$ with the noncyclometalated bisruthenium bridge shows redox events at much positive

dx.doi.org/10.1021/ic400082z | Inorg. Chem. 2013, 52, 4040−4045

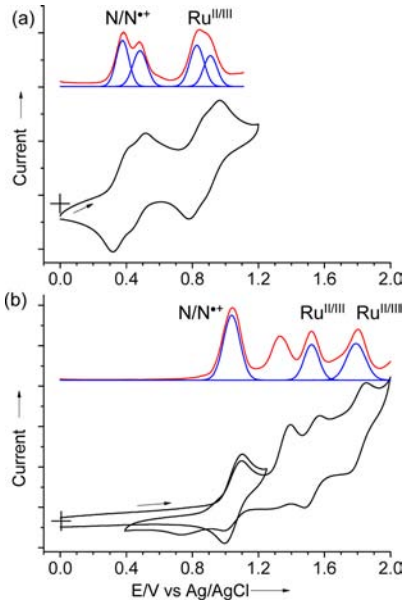

Figure 3. (a) CV (black curve, second potential scan from 0 to +1.2 V) and DPV (red curve) of 2^{2+} with $^{n}Bu_4NB(C_6F_5)_4$ as the supporting electrolyte. (b) CV (black curve, first scan from 0 to +1.2 V and second potential scan from +0.4 to +2.0 V) and DPV (red curve) of 4^{4+} with $^{n}Bu_4NClO_4$ as the supporting electrolyte. The blue lines are the Gaussian-fitted DPV curves.

Table 1. Electrochemical Data[a]

complex	$E_{1/2}$ (V vs Ag/AgCl)
1^{2+}	+0.27, +0.68
2^{2+}[b]	+0.38, +0.48, +0.83, +0.91
2^{2+}	+0.36, +0.46, +0.78 (2e)
3^{2+}	+0.42, +0.54, +0.83, +0.91
4^{4+}	+1.05, +1.33,[c] +1.52, +1.80

[a]If otherwise noted, the electrolyte is $^{n}Bu_4NClO_4$. [b]The electrolyte is $^{n}Bu_4NB(C_6F_5)_4$. [c]Irreversible, E_{peak}.

potentials (Figure 3b). In addition, only one $N/N^{\bullet+}$ process is observed at +1.05 V vs Ag/AgCl. The two ruthenium sites are oxidized at +1.52 and +1.80 V. The intensity ratio between the $N/N^{\bullet+}$ wave and each $Ru^{II/III}$ wave is 2:1, which indicates that the peak at +1.05 V is a two-electron process, and no electronic coupling is present between two distal amine sites in complex 4^{4+}. The irreversible peak at +1.33 V is caused by the further oxidation of the in situ generated aminium intermediate ($N^{\bullet+}/N^{2+}$).[12,14]

Stepwise Oxidation and Spectroscopic Study. To further study the electronic coupling of these compounds, their visible to near-infrared (vis/NIR) absorption spectral changes were monitored and measured upon stepwise chemical oxidation or electrolysis. Figure 4 shows the spectral changes of 2^{2+} upon stepwise oxidations with cerium ammonium nitrate (CAN) in CH_3CN. When up to 1.0 equiv of CAN was added, the ligand-to-ligand charge transfer (LLCT) band at 627 nm decreased. At the same time, a new intense peak at 1125 nm appeared. In accordance with the NIR titration studies of complex 1^{n+},[13] this peak is ascribed to Ru → $N^{\bullet+}$ MNCT transition. No other bands are evident for 2^{3+} up to 2500 nm (Supporting Informaton Figure S5). When up to 2.0 equiv CAN was added (2^{3+} → 2^{4+}), the MNCT band continued to increase. When up to 3.0 and 4.0 equiv of CAN was added (2^{4+} → 2^{5+} → 2^{6+}), the MNCT band gradually decreased. At the same time, a new intense peak at 606 nm appeared. This peak is assigned to the $N^{\bullet+}$ absorption, as has been found in many triaryl aminum cation species.[13,17] Again, no other NIR peak is evident during the oxidation of 2^{4+} to 2^{5+} (Supporting Information Figure S6). In the above four-step process, isosbestic absorption points are clearly visible in each step, for example, 605 and 760 nm in Figure 4a, 580 and 780 nm in Figure 4b, 395 and 780 nm in Figure 4c, and 400 and 664 nm in Figure 4d. This indicates the clean proceeding of these processes.

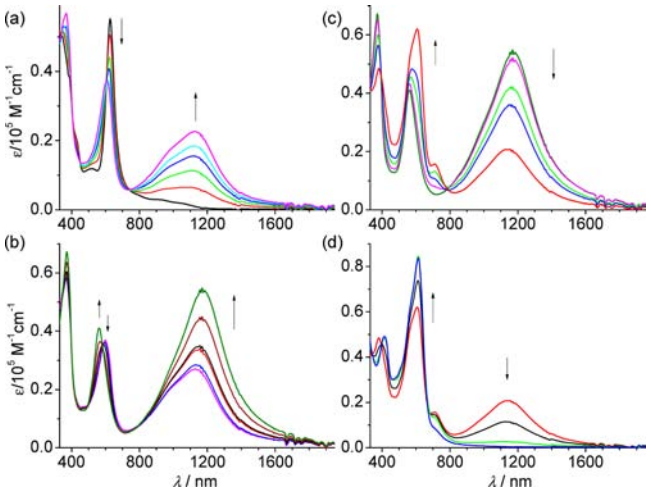

Figure 4. Vis/NIR absorption spectral changes of $[2](PF_6)_2$ in CH_3CN upon stepwise oxidations with gradual addition of CAN up to 1, 2, 3, and 4 equiv for a–d, respectively.

It should be noted that, in Figure 4a and b, an absorption band around 960 nm (as a shoulder) is present. The nature of this band is not clear at this stage. It would be inappropriate to assign this band to the intervalence charge transfer (IVCT) transition between two distal amine sites of 2^{3+}, because the energy of this shoulder band is too high and the absorptivity is too strong for a weakly coupled system.

When complex 2^{2+} was oxidatively titrated with $SbCl_5$ in CH_2Cl_2, which is commonly used in the studies of many bis-triarylamine MV systems,[18] similar four-step spectral changes associated with the stepwise oxidation from 2^{2+} to 2^{6+} are observed (Figure 5a and b). The MNCT band of the singly oxidized state 2^{3+} (1186 nm) are slightly red-shifted relative to that in CH_3CN. In addition, the decrease of the metal-to-ligand charge transfer (MLCT, at 570 nm, Figure 5b) transition is clearly observed during the 2^{4+} → 2^{6+} process, because the $N^{\bullet+}$-associated absorption band is well separated from the MLCT band. In addition, these four-step spectral changes are reproducible by stepwise electrolysis using a transparent indium–tin–oxide (ITO) glass electrode (Figure 5c and d). The applied potentials for these processes are +0.20 → +0.45 → +0.65 → 0.90 → +1.30 V vs Ag/AgCl, which are well correlated with the four redox steps shown in Figure 3.

When the noncyclometalated complex 4^{4+} was oxidized with $SbCl_5$, the emergence of the MNCT band at 1150 nm and the $N^{\bullet+}$-associated absorption at 850 nm were observed (Figure 6).[18] Figure S7 in the Supporting Information shows the vis/NIR absorption spectral changes of 3^{2+} by stepwise oxidation of CAN in CH_3CN. Similarly, a shoulder peak at 950 nm and a MNCT band at 1045 nm are evident for the singly oxidized state 3^{3+}. In the doubly oxidized state 3^{4+}, only one major

dx.doi.org/10.1021/ic400082z | Inorg. Chem. 2013, 52, 4040–4045

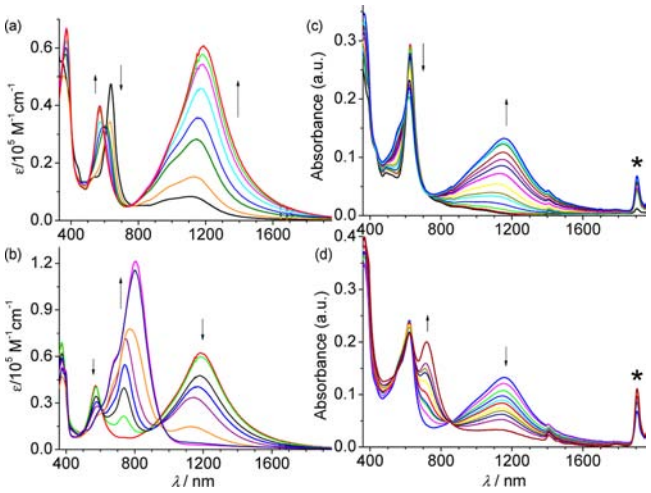

Figure 5. Vis/NIR absorption spectral changes during the (a) $2^{2+} \rightarrow 2^{4+}$ and (b) $2^{4+} \rightarrow 2^{6+}$ process in CH_2Cl_2 upon stepwise oxidation with $SbCl_5$ and during the (c) $2^{2+} \rightarrow 2^{4+}$ and (d) $2^{4+} \rightarrow 2^{6+}$ process in CH_3CN by electrolysis with an ITO glass electrode. The applied potential is +0.20 → +0.65 V and +0.65 → +1.30 V vs Ag/AgCl for (c) and (d), respectively. The different spectral changes of (a, b) with respect to (c, d) are very likely caused by the different solvents used. *: Artifacts.

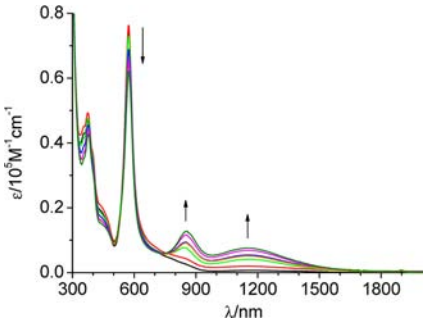

Figure 6. Absorption spectral changes of noncyclometalated complex 4^{4+} in dichloromethane upon oxidation with $SbCl_5$.

MNCT band at 1100 nm was observed and this band decreased upon oxidation to 3^{5+} and 3^{6+}.

Theoretical Calculation and EPR Study. The left plot in Figure 7 displays the EPR spectrum of 2^{3+} generated by the addition of 0.5 equiv of CAN in CH_3CN at room temperature. The singlet signal with a *g* factor of 2.071 is in accordance with the nature of an organic radical species ($N^{\bullet+}$). A low-spin Ru^{III} species is usually EPR inactive at room temperature and sometimes has a rhombic or axial signal at room temperature.[11]

Density functional theory (DFT) calculations were performed on the singly oxidized state 3^{3+} on the level of theory of B3LYP/LANL2DA/6-31G*/vacuum (see details in the Experimental Section) starting from its single-crystal X-ray structure. A spin density evenly distributed over two triarylamines is evident (Figure S8, Supporting Information). However, when the long-range corrected version of B3LYP, CAM-B3LYP,[19] was used, the spin density of 3^{3+} is indeed localized on one triarylamine unit (Figure 7).

Time-dependent DFT (TDDFT) calculations of 3^{3+} were performed at the level of CAM-B3LYP/LanL2DZ/6-31G*/vacuo. The details for the first 10 doublet excitation states are delineated in Table S1 in the Supporting Information. The first state D_1 is predicted at 4682.8 nm with a β-highest occupied spin orbital (HOSO) → β-lowest unoccupied spin orbital (LUSO) character and with low oscillator strength (f) of 0.0002. This excitation can be interpreted as the IVCT transition between two distal amine sites (the spin orbitals are shown in Supporting Information Figures S9 and S10). The D_3 state at 1714.0 nm (f = 0.0001) and D_5 state at 1229.5 nm (f = 0.0015) are both associated with the LLCT transitions from the triarylamine unit to the tppz ligand. The D_6 state at 1042.5 nm with f = 0.0007 has major contribution from the $ML_{tppz}CT$ transitions. These LLCT and MLCT transitions are possibly buried inside the experimentally observed MNCT transitions. The D_7 state at 854.3 nm with a high f value (0.6539) is associated with the MNCT transitions with the character of β-HOSO-8 → β-LUSO excitation. Other excitations have f = 0.

The above TDDFT results do not suggest the presence of the shoulder band at 960 nm of 2^{3+} in Figure 4. The failure to experimentally observe the IVCT band is possibly because the IVCT band is at a very low-energy region, as suggested by the TDDFT calculations (4682.8 nm). Another possibility is that the weak IVCT band, if present, might be buried inside the intense MNCT band in the NIR region. Nevertheless, the distinct potential splitting between two $N/N^{\bullet+}$ processes is solid evidence of the amine−amine coupling through the cyclometalated bisruthenium segment.

CONCLUSIONS

In conclusion, a four-center redox-active system with a linear N−Ru−Ru−N array has been successfully synthesized and characterized with single-crystal X-ray analysis. This system displays four consecutive and well-separated redox waves at low potentials. Electrochemical studies support the presence of amine−amine electronic coupling with a distance of 19.16 Å through the cyclometalated bisruthenium segment. This

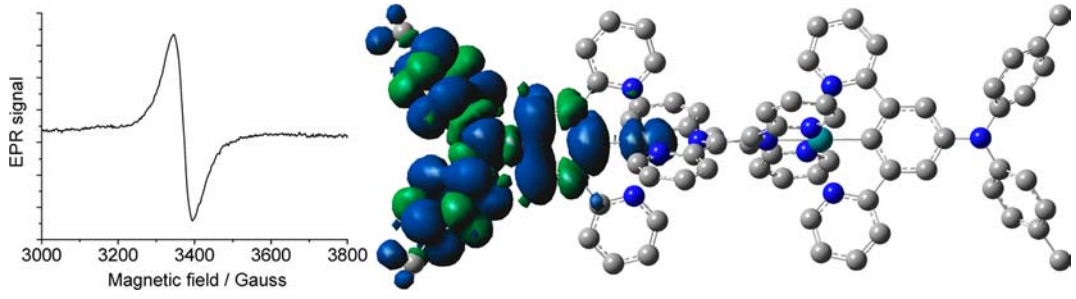

Figure 7. Left: EPR signal at room temperature of 2^{3+} generated by the addition of 0.5 equiv of CAN. Right: Spin density plot of 3^{3+} calculated with CAM-B3LYP/LANL2DA/6-31G*/vacuum. Hydrogen atoms are omitted for clarity.

dx.doi.org/10.1021/ic400082z | Inorg. Chem. 2013, 52, 4040−4045

provides a new concept for the design of highly conductive one-dimensional molecular wires.[1,2] In addition, the significantly different NIR spectral changes with intensities as high as 54000 M^{-1} cm^{-1} in response to external electrochemical stimulus will make these materials potentially useful for charge-based information storage[3] and electrochromic devices.[20]

EXPERIMENTAL SECTION

Spectroscopic Measurements. Spectroelectrochemical measurements were performed in a thin-layer cell (optical length 0.2 cm) in which an ITO glass electrode was set in the indicated solvent containing the compound to be studied (the concentration is around 1 × 10^{-4} M) and 0.1 M Bu_4NClO_4 as the supporting electrolyte. A platinum wire and Ag/AgCl in saturated aqueous NaCl solution was used as the counter electrode and reference electrode, respectively. The cell was put into a PE Lambda 750 UV/vis/NIR spectrophotometer to monitor spectral changes during electrolysis. During the measurement with chemical oxidation, different equivalent of oxidant (CAN in CH_3CN or $SbCl_5$ in CH_2Cl_2) were added to a solution of the compound in study with constant concentration. The obtained solution was measured by the UV/vis/NIR spectrophotometer.

Electrochemical Measurements. All CV and DPV measurements were taken using a CHI620D potentiostat with one-compartment electrochemical cell under an atmosphere of nitrogen. All measurements were carried out in 0.1 M of $^n Bu_4NClO_4$ or $^n Bu_4NB(C_6F_5)_4$ in CH_3CN at a scan rate of 100 mV/s. $^n Bu_4NB(C_6F_5)_4$ was synthesized according to know procedure.[16] The working electrode was a glassy carbon with a diameter of 0.3 mm. The electrode was polished prior to use with 0.05 μm alumina and rinsed thoroughly with water and acetone. A large area platinum wire coil was used as the counter electrode. All potentials are referenced to a Ag/AgCl electrode in saturated aqueous NaCl without regard for the liquid junction potential. Figure S11 in the Supporting Information shows the DPV of $\mathbf{2}^{2+}$ in the presence of ferrocene (Fc) as the internal standard. The $Fc^{0/+}$ signal overlaps with one $N^{0/+}$ peak. The potential vs $Fc^{0/+}$ can be estimated from that versus Ag/AgCl by subtracting 0.45 V.

X-ray Crystallography. The X-ray diffraction data were collected using a Rigaku Saturn 724 diffractometer on a rotating anode (Mo K radiation, 0.71073 Å) at 173 K. The structure was solved by the direct method using SHELXS-97[21] and refined with Olex2.[22] The structure graphic shown in shown in Figure 2 was generated using Olex2. Crystallographic data for $[\mathbf{3}](BPh_4)_2$: $C_{132}H_{104}B_2N_{12}Ru_2$, M = 2082.03, monoclinic, space group $C2/c$, a = 38.070(8) Å, b = 11.795(2) Å, c = 26.950(5) Å, α = 90°, β = 105.76(3)°, γ = 90°, U = 11647(4) Å^3, T = 173 K, Z = 4, 12 457 reflections measured, radiation type Mo Kα, radiation wavelength 0.71073 Å, final R indices R1 = 0.1364, wR2 = 0.2892, R indices (all data) R1 = 0.1878, wR2 = 0.3204. CCDC 917533 contains the supplementary crystallographic data for this paper. These data can be obtained free of charge from The Cambridge Crystallographic Data Centre via www.ccdc.cam.ac.uk/data_request/cif.

Computational Methods. DFT calculations are carried out using the B3LYP[23] or CAM-B3LYP[19] exchange correlation functional and implemented in the *Gaussian* 09 package.[24] The electronic structures of complexes were determined using a general basis set with the Los Alamos effective core potential LanL2DZ basis set for ruthenium, and 6-31G* for other atoms[25] In case of the solvation effects (acetonitrile) are included, the conductor-like polarizable continuum model (CPCM) was employed.[26] All orbitals have been computed at an isovalue of 0.02 e/bohr.[3]

Synthesis. NMR spectra were recorded in the designated solvent on Bruker Avance 400 MHz spectrometer. Spectra are reported in ppm values from residual protons of deuterated solvent. Mass data were obtained with a Bruker Daltonics Inc. Apex II FT-ICR or Autoflex III MALDI-TOF mass spectrometer. The matrix for MALDI-TOF measurement is α-cyano-4-hydroxycinnamic acid. Microanalysis was carried out using Flash EA 1112 or Carlo Erba 1106 analyzer at the Institute of Chemistry, Chinese Academy of Sciences.

Synthesis of $[\mathbf{2}](PF_6)_2$. To 20 mL of dry acetone were added $[RuCl_3(tppz)RuCl_3]$[14] (0.030 mmol, 24.0 mg) and AgOTf (0.20 mmol, 52.0 mg). The mixture was refluxed for 3 h before it was cooled to room temperature. After the mixture stood at room temperature for around one hour, the resulting AgCl precipitate was removed by filtration. The filtrate was concentrated to dryness. To the residue were added 1-(di-*p*-anisylamino)-3,5-di(2-pyridyl)benzene[13] (0.060 mmol, 27.6 mg), 10 mL DMF, and10 mL ^{t}BuOH. The mixture was bubbled with nitrogen for 20 min before the vial was capped and heated at 130 °C for 48 h. After the mixture was cooled to room temperature, the solvent was removed under reduced pressure. The residue was dissolved in 2 mL methanol, followed by the addition of an excess of aq. KPF_6. The resulting precipitate was collected by filtering and washing with water and Et_2O. The obtained solid was purified by chromatography on silica gel (eluent CH_3CN/H_2O/aq. KNO_3 120/30/0.1), followed by anion exchange using KPF_6, to give 24.0 mg of the bisruthenium complex $\mathbf{2}^{2+}$ as a black solid in 45% yield. MALDI-MS: 1506.8 for $[M - 2PF_6]^+$. Anal. Calcd for $C_{84}H_{64}F_{12}N_{12}O_4P_2Ru_2 \cdot 6H_2O$: C, 52.94; H, 4.02; N, 8.82. Found: C, 52.58; H, 3.85; N, 8.32.

Synthesis of $[\mathbf{3}](PF_6)_2$. To a solution of 3,5-di(2-pyridyl)-bromobenzene[13] (1.0 mmol, 323 mg) and 4,4′-dimethyldiphenylamine (1.5 mmol, 296 mg) in 20 mL dry toluene were added $Pd_2(dba)_3$ (0.02 mmol, 18.3 mg), 1,1′-bis(diphenylphosphino)ferrocene (dppf) (0.020 mmol, 11.1 mg) and NaO^{t}Bu (1.2 mmol, 115.3 mg) under a N_2 atmosphere. The mixture was bubbled with nitrogen for 10 min before the vial was capped and heated at 130 °C for 48 h. After cooling to room temperature, the solvent was removed under reduced pressure. The residue was then subjected to column chromatography on silica gel (eluent: CH_2Cl_2/ethyl acetate, 10/1) to afford 215 mg of 1-(di-*p*-tolylamino)-3,5-di(2-pyridyl)benzene as a yellow solid in 50% yield. ^{1}H NMR (400 MHz, $CDCl_3$): δ 2.30 (s, 6H), 7.05 (s, 8H), 7.20 (m, 2H), 7.70 (m, 4H), 7.72 (s, 2H), 8.20 (s, 1H), 8.63 (d, J = 6.3 Hz, 2H). ^{13}C NMR (100 MHz, $CDCl_3$): δ 20.8, 119.6, 120.9, 122.2, 122.3, 124.4, 129.9, 132.3, 136.7, 140.9, 145.4, 149.3, 149.4, 157.2. EI-MS (m/z): 427 $[M]^+$. EI-HRMS: calcd for $C_{30}H_{25}N_3$ 427.2048, found 427.2055.

According to the same procedure for the synthesis of $[\mathbf{2}](PF_6)_2$, complex $[\mathbf{3}](PF_6)_2$ was prepared from $[RuCl_3(tppz)RuCl_3]$ (0.030 mmol, 24.0 mg) and the above prepared 1-(di-*p*-tolylamino)-3,5-di(2-pyridyl)benzene (0.060 mmol, 26.0 mg) in a yield of 38% (20.0 mg of $[\mathbf{3}](PF_6)_2$ was isolated). MALDI-MS: 1443.2 for $[M - 2PF_6]^+$. Anal. Calcd for $C_{84}H_{64}F_{12}N_{12}P_2Ru_2 \cdot H_2O$: C, 57.60; H, 3.80; N, 9.60. Found: C, 57.23; H, 3.87; N, 9.35.

Synthesis of $[\mathbf{4}](PF_6)_4$. A mixture of $[RuCl_3(tppz)RuCl_3]$ (0.10 mmol, 80.3 mg) and 4′-di-*p*-anisylamino-2,2′:6′,2″-terpyridine[12c] (0.21 mmol, 96.7 mg) in 5 mL of ethylene glycol were heated under under microwave conditions (power = 375 W) for 30 min. After the mixture was cooled to room temperature, an excess of aqueous KPF_6 solution were added. The resulting precipitate was collected by filtering and washing successively with water and ether. The crude product was purified by flash column chromatography on silica gel using 30/1/0.05 acetonitrile/water/saturated KNO_3 as the eluent. After anion exchange using KPF_6, 69 mg of complex $[\mathbf{4}](PF_6)_4$ was obtained as a black solid in a yield of 33%. ^{1}H NMR (400 MHz, CD_3CN): δ 3.90 (s, 12 H), 7.14−7.20 (m, 12 H), 7.46 (t, J = 6.54 Hz, 4 H), 7.57 (d, J = 8.7 Hz, 8 H), 7.82 (t, J = 7.8 Hz, 4 H), 7.88−7.95 (m, 16 H), 8.16 (d, J = 8.0 Hz, 4 H), 8.91 (d, J = 8.3 Hz, 4 H). MALDI-TOF (m/z): 1653.0 for $[M - 3PF_6]^+$, 1509.0 for $[M - 4PF_6]^+$. Anal. Calcd for $C_{82}H_{64}F_{24}N_{14}O_4P_4Ru_2 \cdot 2CH_3CN$: C, 47.52; H, 3.25; N, 10.32. Found: C, 47.96; H, 3.37; N, 10.18.

ASSOCIATED CONTENT

Supporting Information

CV, oxidative titration, DFT, and TDDFT results, NMR and MS spectra, and CIF file for $[\mathbf{3}](BPh_4)_2$. This material is available free of charge via the Internet at http://pubs.acs.org.

dx.doi.org/10.1021/ic400082z | Inorg. Chem. 2013, 52, 4040−4045

AUTHOR INFORMATION

Corresponding Author

*E-mail: zhongyuwu@iccas.ac.cn.

Notes

The authors declare no competing financial interest.

ACKNOWLEDGMENTS

This work is supported by the National Natural Science Foundation of China (grants 21271176, 91227104, 21002104, and 212210017), the National Basic Research 973 program of China (grant 2011CB932301), and Institute of Chemistry, Chinese Academy of Sciences ("100 Talent Program" and grant CMS-PY-201230). Si-Hai Wu of the same research group is acknowledged for the synthesis of $^{n}Bu_4NB(C_6F_5)_4$.

REFERENCES

(1) (a) D'Alessandro, D. M.; Keene, F. R. *Chem. Rev.* **2006**, *106*, 2270. (b) Kaim, W.; Lahiri, G. K. *Angew. Chem., Int. Ed.* **2007**, *46*, 1778. (c) Flores-Torres, S.; Hutchison, G. R.; Stoltzberg, L. J.; Abruna, H. D. *J. Am. Chem. Soc.* **2006**, *128*, 1513. (d) Lincke, K.; Frellsen, A. F.; Parkar, C. R.; Bond, A. D.; Hammerich, O.; Nielsen, M. B. *Angew. Chem., Int. Ed.* **2012**, *51*, 6099.

(2) (a) Tuccitto, N.; Ferri, V.; Cavazzini, M.; Quici, S.; Zhavnerko, G.; Licciardello, A.; Rampi, M. A. *Nat. Mater.* **2009**, *8*, 41. (b) Ying, J.-W.; Liu, I. P.-C.; Xi, B.; Song, Y.; Campana, C.; Zuo, J.-L.; Ren, T. *Angew. Chem., Int. Ed.* **2010**, *49*, 954. (c) Kurita, T.; Nishimori, Y.; Toshimitsu, F.; Muratsugu, S.; Kume, S.; Nishihara, H. *J. Am. Chem. Soc.* **2010**, *132*, 4524.

(3) (a) Lindsey, J. S.; Bocian, D. F. *Acc. Chem. Res.* **2011**, *44*, 638. (b) Simao, C.; Mas-Torrent, M.; Crivillers, N.; Lloveras, V.; Artes, J. M.; Gorostiza, P.; Veciana, J.; Rovira, C. *Nat. Chem.* **2011**, *3*, 359.

(4) (a) Launay, J.-P. *Chem. Soc. Rev.* **2001**, *30*, 386. (b) Wenger, O. S. *Acc. Chem. Res.* **2011**, *44*, 25. (c) Flamigni, L.; Collin, J.-P.; Sauvage, J.-P. *Acc. Chem. Res.* **2008**, *41*, 857.

(5) (a) Nelsen, S. E. *Chem.—Eur. J.* **2000**, *6*, 581. (b) Hankache, J.; Wenger, O. S. *Chem. Rev.* **2011**, *111*, 5138. (c) Chisholm, M. H.; Lear, B. J. *Chem. Soc. Rev.* **2011**, *40*, 5254. (d) Heckmann, S.; Lambert, C. *Angew. Chem., Int. Ed.* **2012**, *51*, 326 and references therein.

(6) (a) Creutz, C.; Taube, H. *J. Am. Chem. Soc.* **1969**, *91*, 3988. (b) Creutz, C.; Taube, H. *J. Am. Chem. Soc.* **1973**, *95*, 1086.

(7) (a) Djukic, J.-P.; Sortais, J.-B.; Barloy, L.; Pfeffer, M. *Eur. J. Inorg. Chem.* **2009**, 817. (b) Gagliardo, M.; Snelders, D. J. M.; Chase, P. A.; Gebbink, R. J. M. K.; van Klink, G. P. M.; van Koten, G. *Angew. Chem., Int. Ed.* **2007**, *46*, 8558.

(8) (a) Bomben, P. G.; Robson, K. C. D.; Sedach, P. A.; Berlinguette, C. P. *Inorg. Chem.* **2009**, *48*, 9631. (b) Wadman, S. H.; Lutz, M.; Tooke, D. M.; Spek, A. L.; Hartl, F.; Havenith, R. W. A.; van Klink, G. P. M.; van Koten, G. *Inorg. Chem.* **2009**, *48*, 1887. (c) Yang, W.-W.; Wang, L.; Zhong, Y.-W.; Yao, J. *Organometallics* **2011**, *30*, 2236. (d) Coudret, C.; Fraysse, S.; Launay, J.-P. *Chem. Commun.* **1998**, 663. (e) Zhong, Y.-W.; Wu, S.-H.; Burkhardt, S. E.; Yao, C.-J.; Abruña, H. D. *Inorg. Chem.* **2011**, *50*, 517.

(9) (a) Wadman, S. H.; Kroom, J. M.; Bakker, K.; Lutz, M.; Spek, A. L.; van Klink, G. P. M.; van Koten, G. *Chem. Commun.* **2007**, 1907. (b) Bomben, P. G.; Robson, K. C. D.; Koivisto, B. D.; Berlinguette, C. P. *Coord. Chem. Rev.* **2012**, *256*, 1438 and references therein.

(10) (a) Patoux, C.; Launay, J.-P.; Beley, M.; Chodorowski-Kimmers, S.; Collin, J.-P.; James, S.; Sauvage, J.-P. *J. Am. Chem. Soc.* **1998**, *120*, 3717. (b) Fraysse, S.; Coudret, C.; Launay, J.-P. *J. Am. Chem. Soc.* **2003**, *125*, 5880. (c) Wadman, S. H.; Havenith, R. W. A.; Hartl, F.; Lutz, M.; Spek, A. L.; van Klink, G. P. M.; van Koten, G. *Inorg. Chem.* **2009**, *48*, 5685.

(11) (a) Yao, C.-J.; Zhong, Y.-W.; Yao, J. *J. Am. Chem. Soc.* **2011**, *133*, 15697. (b) Shao, J.-Y.; Yang, W.-W.; Yao, J.; Zhong, Y.-W. *Inorg. Chem.* **2012**, *52*, 4343. (c) Sui, L.-Z.; Yang, W.-W.; Yao, C.-J.; Xie, H.-Y.; Zhong, Y.-W. *Inorg. Chem.* **2012**, *51*, 1590.

(12) (a) Nie, H.-J.; Chen, X.; Yao, C.-J.; Zhong, Y.-W.; Hutchison, G. R.; Yao, J. *Chem.—Eur. J.* **2012**, *18*, 14497. (b) Zhang, Y.-M.; Wu, S.-H.; Yao, C.-J.; Nie, H.-J.; Zhong, Y.-W. *Inorg. Chem.* **2012**, *51*, 11387. (c) Yao, C.-J.; Yao, J.; Zhong, Y.-W. *Inorg. Chem.* **2011**, *50*, 6847.

(13) Yao, C.-J.; Zheng, R.-H.; Shi, Q.; Zhong, Y.-W.; Yao, J. *Chem. Commun.* **2012**, *48*, 5680.

(14) Hartshom, C. M.; Daire, N.; Tondreau, V.; Loeb, B.; Meyer, T. J.; White, P. S. *Inorg. Chem.* **1999**, *38*, 3200.

(15) (a) Yang, W.-W.; Zhong, Y.-W.; Yoshikawa, S.; Shao, J.-Y.; Masaoka, S.; Sakai, K.; Yao, J.; Haga, M.-a. *Inorg. Chem.* **2012**, *51*, 890. (b) Zhang, Y.-M.; Shao, J.-Y.; Yao, C.-J.; Zhong, Y.-W. *Dalton Trans.* **2012**, *41*, 9280.

(16) (a) LeSuer, R. J.; Geiger, W. E. *Angew. Chem., Int. Ed.* **2000**, *39*, 248. (b) Geiger, W. E.; Barriere, F. *Acc. Chem. Res.* **2010**, *43*, 1030. (c) LeSuer, R.; Bettolph, C.; Geiger, W. E. *Anal. Chem.* **2004**, *76*, 6395.

(17) (a) Sreenath, K.; Thomas, T. G.; Gopidas, K. R. *Org. Lett.* **2011**, *13*, 1134. (b) Sakamaki, D.; Ito, A.; Tanaka, K.; Furukawa, K.; Kato, T.; Shiro, M. *Angew. Chem., Int. Ed.* **2012**, *51*, 8281.

(18) (a) Lambert, C.; Nöll, G. *J. Am. Chem. Soc.* **1999**, *121*, 8434. (b) Lambert, C.; Nöll, G.; Schelter, J. *Nat. Mater.* **2002**, *1*, 69. (c) Jones, S. C.; Coropceanu, V.; Barlow, S.; Kinnibrugh, T.; Timofeeva, T.; Brédas, J.-L.; Marder, S. R. *J. Am. Chem. Soc.* **2004**, *126*, 11782. (d) Lambert, C.; Risko, C.; Coropceanu, V.; Schelter, J.; Amthor, S.; Gruhn, N. E.; Durivage, J. C.; Brédas, J.-L. *J. Am. Chem. Soc.* **2005**, *127*, 8508. (e) Heckmann, A.; Amothor, S.; Lambert, C. *Chem. Commun.* **2006**, 2959.

(19) Yanai, T.; Tew, D. P.; Handy, N. C. *Chem. Phys. Lett.* **2004**, *393*, 51.

(20) (a) Yao, C.-J.; Zhong, Y.-W.; Nie, H.-J.; Abruna, H. D.; Yao, J. *J. Am. Chem. Soc.* **2011**, *133*, 20720. (b) Kaim, W. *Coord. Chem. Rev.* **2011**, *255*, 2503.

(21) Sheldrick, G. M. *Acta Crystallogr.* **2008**, *A64*, 112.

(22) Dolomanov, O. V.; Bourhis, L. J.; Gildea, R. J.; Howard, J. A. K.; Puschmann, H. *J. Appl. Crystallogr.* **2009**, *42*, 339.

(23) (a) Becke, A. D. *J. Chem. Phys.* **1993**, *98*, 5648. (b) Lee, C.; Yang, W.; Parr, R. G. *Phys. Rev. B* **1988**, *37*, 785.

(24) Frisch, M. J.; Trucks, G. W.; Schlegel, H. B.; Scuseria, G. E.; Robb, M. A.; Cheeseman, J. R.; Montgomery, J. A.; Vreven, Jr. T.; Kudin, K. N.; Burant, J. C.; Millam, J. M.; Iyengar, S. S.; Tomasi, J.; Barone, V.; Mennucci, B.; Cossi, M.; Scalmani, G.; Rega, N.; Petersson, G. A.; Nakatsuji, H.; Hada, M.; Ehara, M.; Toyota, K.; Fukuda, R.; Hasegawa, J.; Ishida, M.; Nakajima, T.; Honda, Y.; Kitao, O.; Nakai, H.; Klene, M.; Li, X.; Knox, J. E.; Hratchian, H. P.; Cross, J. B.; Adamo, C.; Jaramillo, J.; Gomperts, R.; Stratmann, R. E.; Yazyev, O.; Austin, A. J.; Cammi, R.; Pomelli, C.; Ochterski, J. W.; Ayala, P. Y.; Morokuma, K.; Voth, G. A.; Salvador, P.; Dannenberg, J. J.; Zakrzewski, V. G.; Dapprich, S.; Daniels, A. D.; Strain, M. C.; Farkas, O.; Malick, D. K.; Rabuck, A. D.; Raghavachari, K.; Foresman, J. B.; Ortiz, J. V.; Cui, Q.; Baboul, A. G.; Clifford, S.; Cioslowski, J.; Stefanov, B. B.; Liu, G.; Liashenko, A.; Piskorz, P.; Komaromi, I.; Martin, R. L.; Fox, D. J.; Keith, T.; Al-Laham, M. A.; Peng, C. Y.; Nanayakkara, A.; Challacombe, M.; Gill, P. M. W.; Johnson, B.; Chen, W.; Wong, M. W.; Gonzalez, C.; Pople, J. A. *Gaussian 09*, revision A.2; Gaussian, Inc.: Wallingford CT, 2009.

(25) (a) Dunning, T. H.; Hay, P. J. In *Modern Theoretical Chemistry*; Schaefer, H. F., Ed.; Plenum: New York, 1976; Vol. 3, p 1. (b) Hay, P. J.; Wadt, W. R. *J. Chem. Phys.* **1985**, *82*, 270. (c) Wadt, W. R.; Hay, P. J. *J. Chem. Phys.* **1985**, *82*, 284. (d) Hay, P. J.; Wadt, W. R. *J. Chem. Phys.* **1985**, *82*, 299.

(26) (a) Klamt, A.; Schüürmann, G. *J. Chem. Soc., Perkin Trans. 2* **1993**, 799. (b) Andzelm, J.; Kölmel, C.; Klamt, A. *J. Chem. Phys.* **1995**, *103*, 9312. (c) Barone, V.; Cossi, M. *J. Phys. Chem. A* **1998**, *102*, 1995. (d) Cossi, M.; Rega, N.; Scalmani, G.; Barone, V. *J. Comput. Chem.* **2003**, *24*, 669. (e) Takano, Y.; Houk, K. N. *J. Chem. Theory Comput.* **2005**, *1*, 70.